

Visible-light-driven photocatalysis of carbon dioxide and organic pollutants by $\text{CaBiO}_2\text{X/g-C}_3\text{N}_4$ (X = Cl, Br)

科學教育與應用學系 四年級 黃柏衡
指導教授 陳錦章 卓越講座教授兼理學院院長

Abstract

Solar-driven photocatalysis is an emerging research field because it offers the potential to mitigate the greenhouse effect on Earth and reduce environmental pollution by converting carbon dioxide into solar fuels and degrading organic pollutants through photocatalysts. We have successfully synthesized calcium bismuth oxyhalide for the first time and investigated its photocatalytic performance in CO_2 reduction and organic pollutant degradation. It exhibits rapid charge carrier separation efficiency and high light absorption capacity, representing a novel photocatalyst. In this study, a new heterogeneous calcium bismuth oxyhalide was synthesized using a High Temperature Calcination Method in a high-temperature furnace. Subsequently, different proportions of graphite nitride were combined to find the optimal efficiency photocatalyst for the photocatalytic reduction of CO_2 and the degradation of the dye Rhodamine 6G (Rh6G). By employing methods to reduce the recombination rate of catalyst electrons and holes, we aimed to enhance the efficiency of CO_2 reduction and pollutant degradation. Additionally, we explored the photocatalytic activity and mechanisms of the prepared catalyst.

Results and Discussion

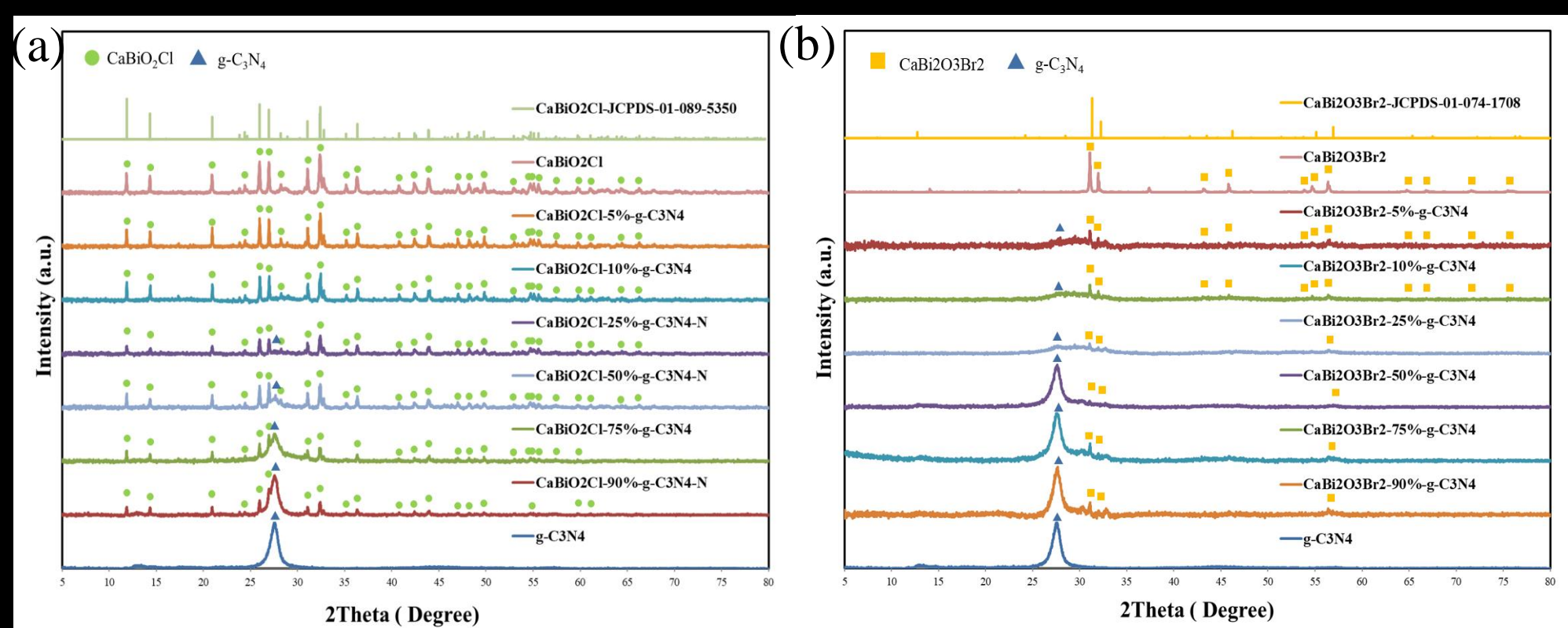


Figure 1. XRD patterns of as-prepared (a) $\text{CaBiO}_2\text{Cl/g-C}_3\text{N}_4$ and (b) $\text{CaBi}_2\text{O}_3\text{Br}_2/\text{g-C}_3\text{N}_4$ samples.

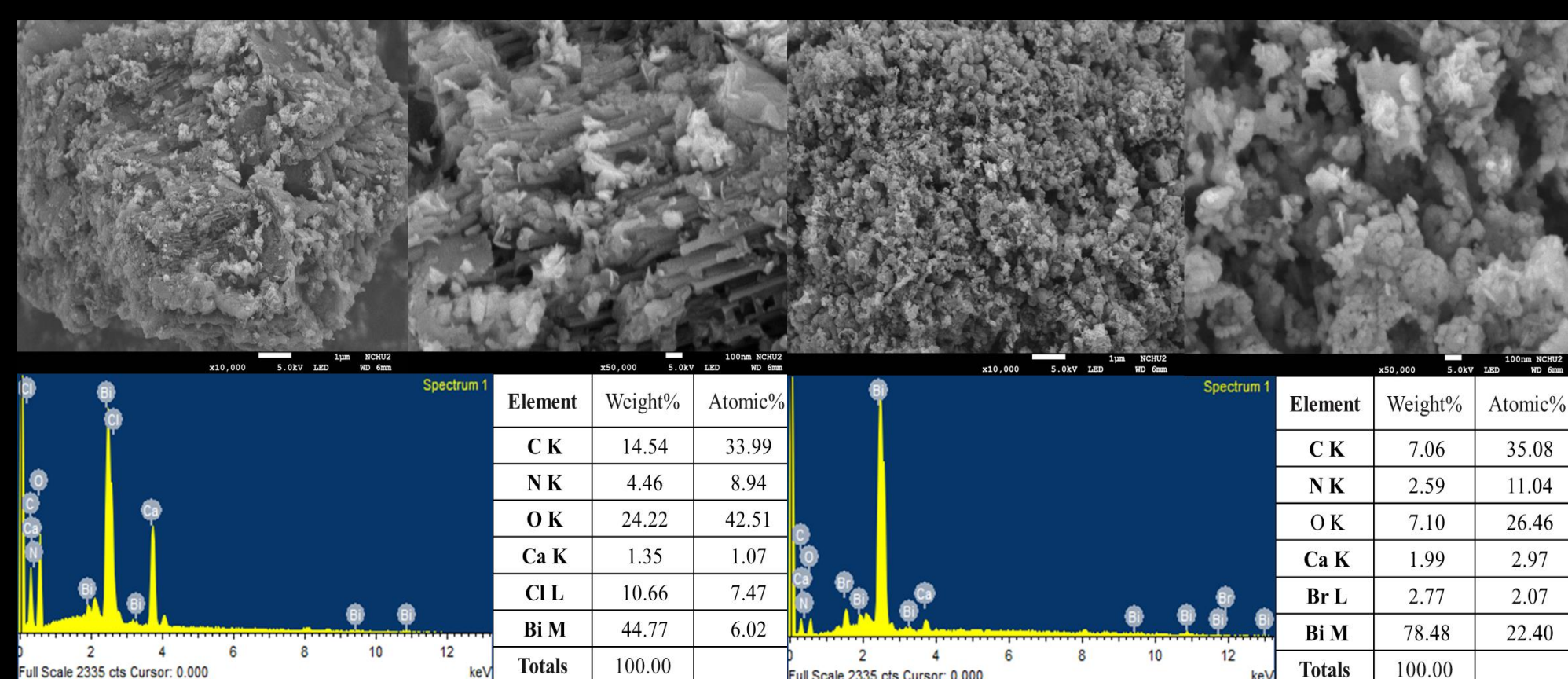


Figure 2. FE-SEM images and EDS of (a) $\text{CaBiO}_2\text{Cl/g-C}_3\text{N}_4$ and (b) $\text{CaBi}_2\text{O}_3\text{Br}_2/\text{g-C}_3\text{N}_4$.

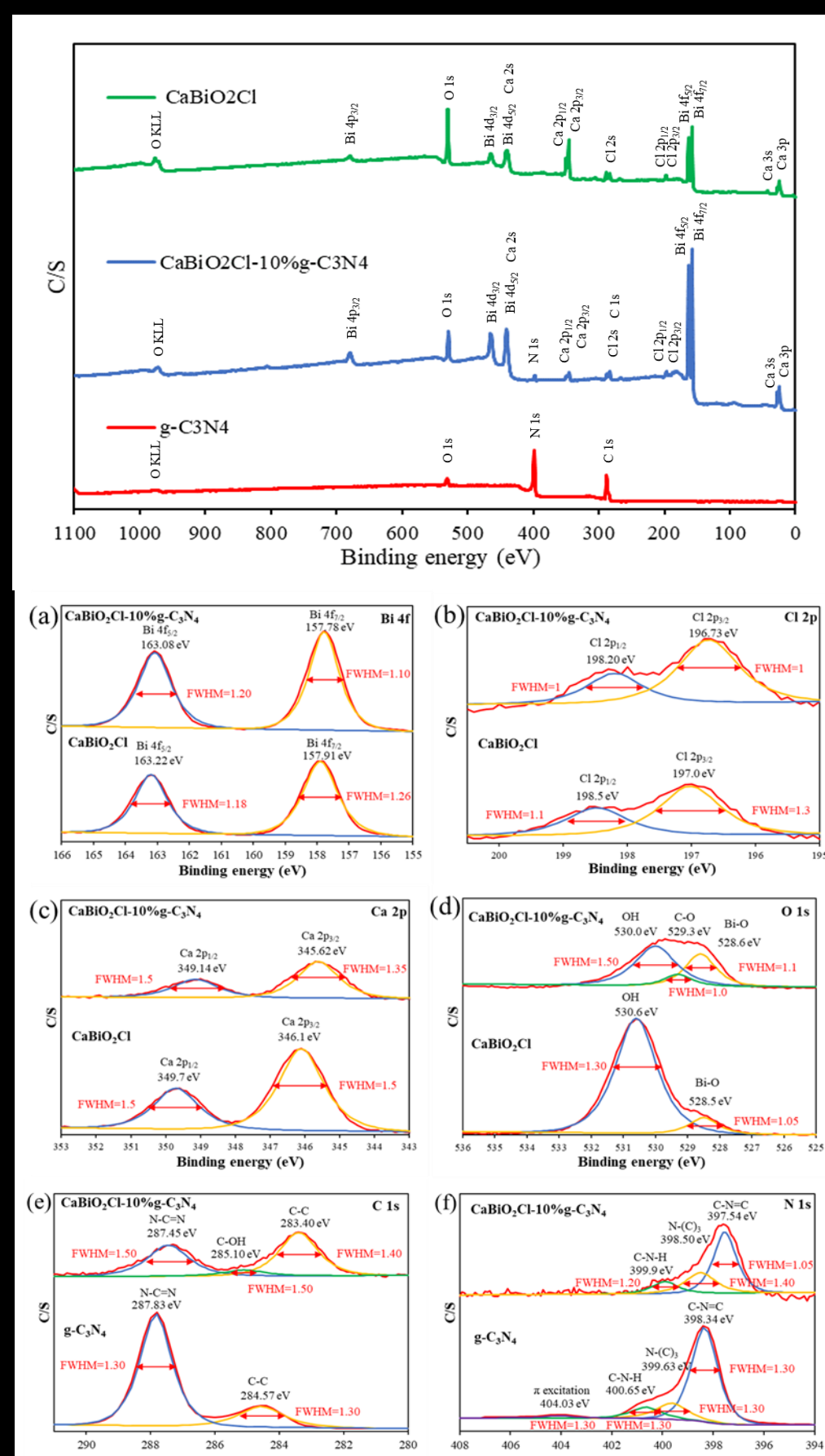


Figure 3. HR-XPS pattern of CaBiO_2Cl sample.

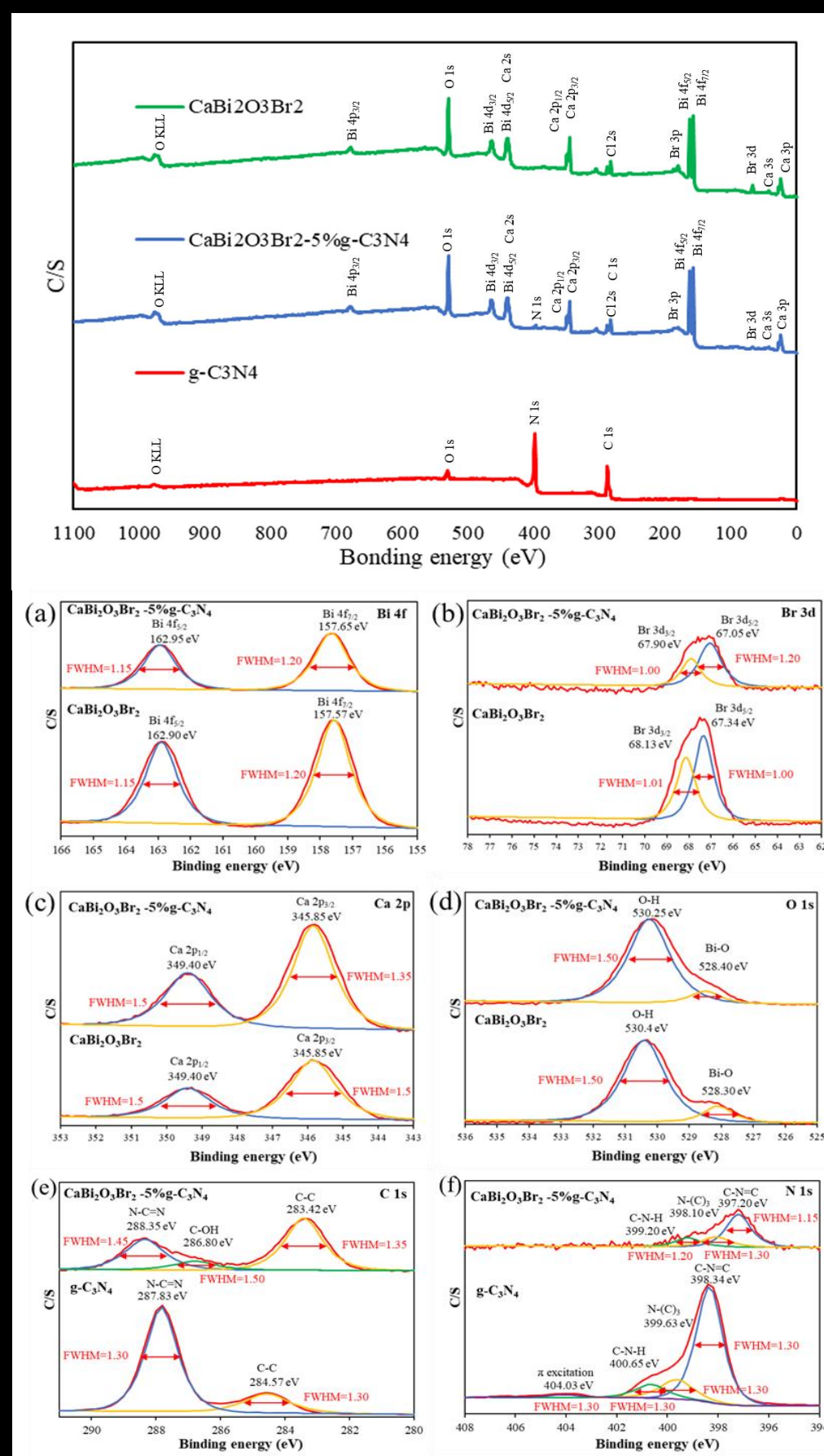


Figure 4. HR-XPS pattern of $\text{CaBi}_2\text{O}_3\text{Br}_2$ sample.

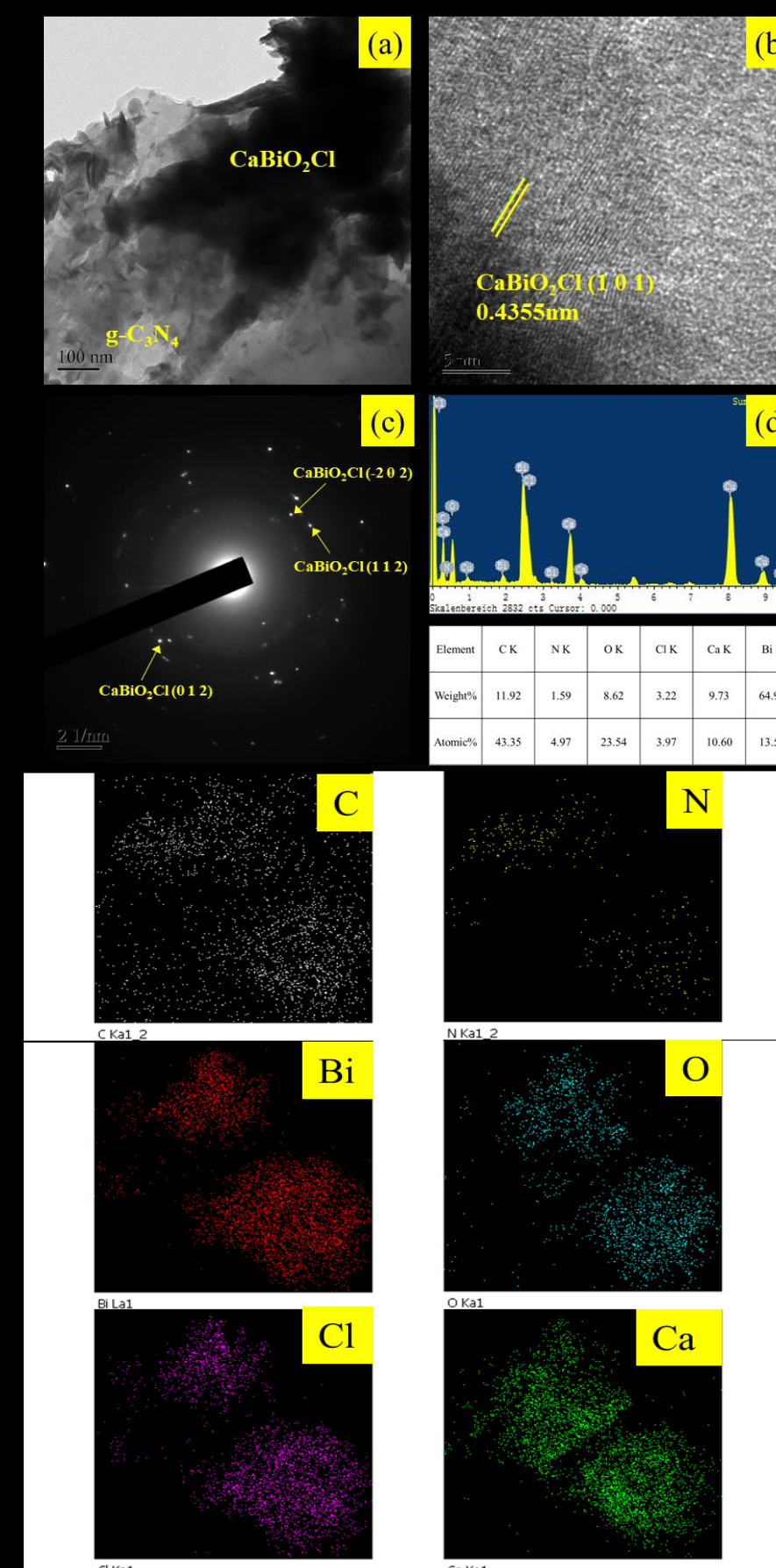


Figure 5. TEM images $\text{CaBiO}_2\text{Cl/g-C}_3\text{N}_4$.

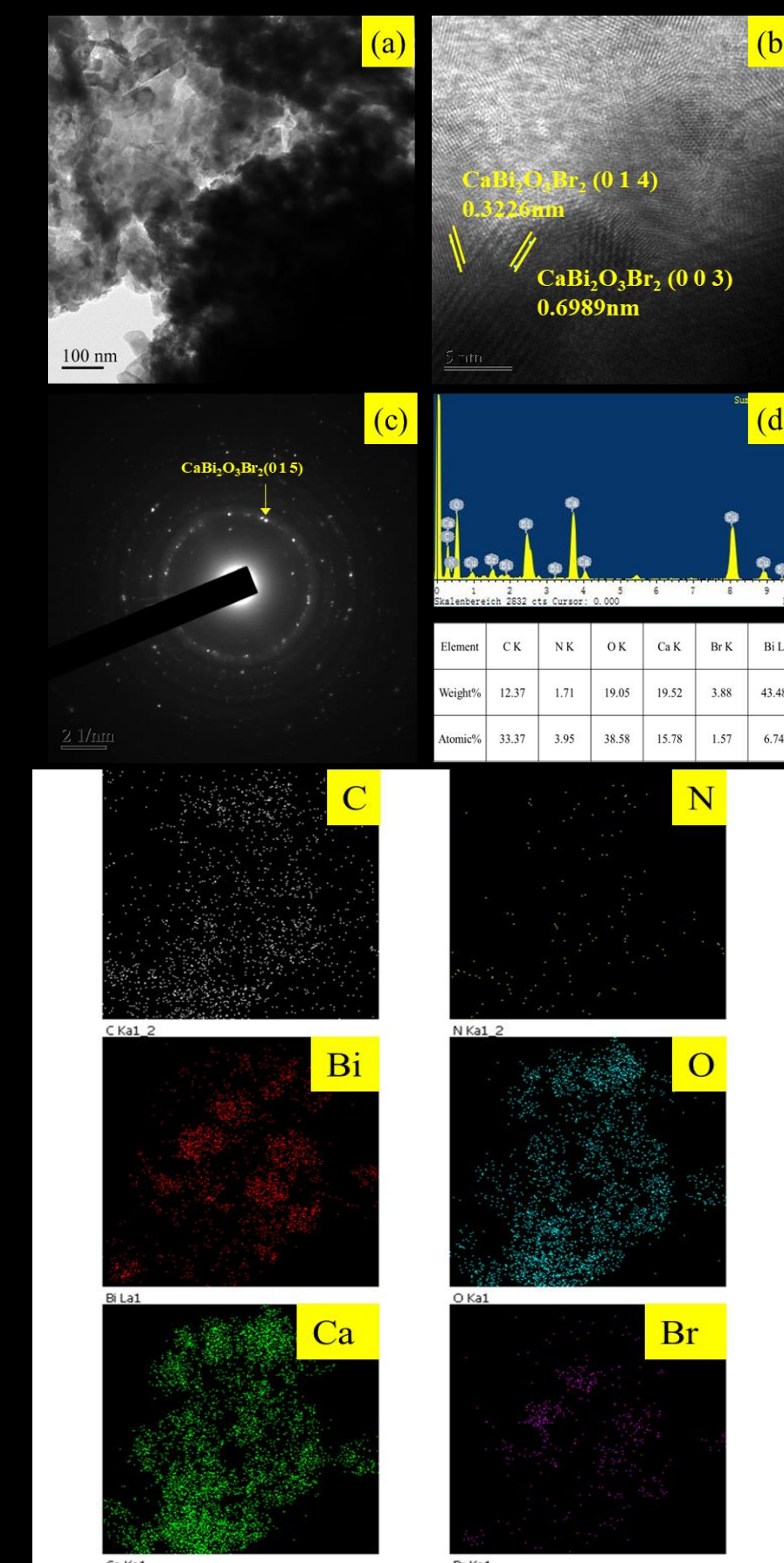


Figure 6. TEM images $\text{CaBi}_2\text{O}_3\text{Br}_2/\text{g-C}_3\text{N}_4$.

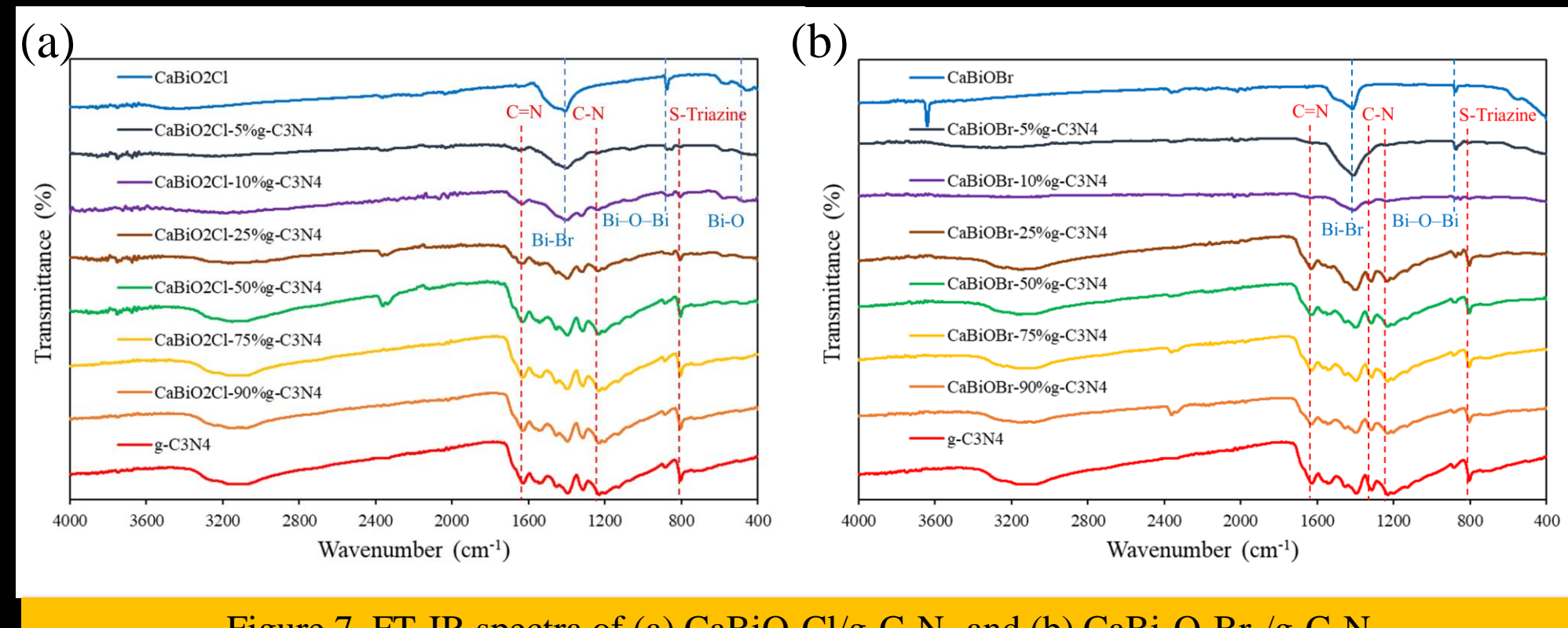


Figure 7. FT-IR spectra of (a) $\text{CaBiO}_2\text{Cl/g-C}_3\text{N}_4$ and (b) $\text{CaBi}_2\text{O}_3\text{Br}_2/\text{g-C}_3\text{N}_4$.

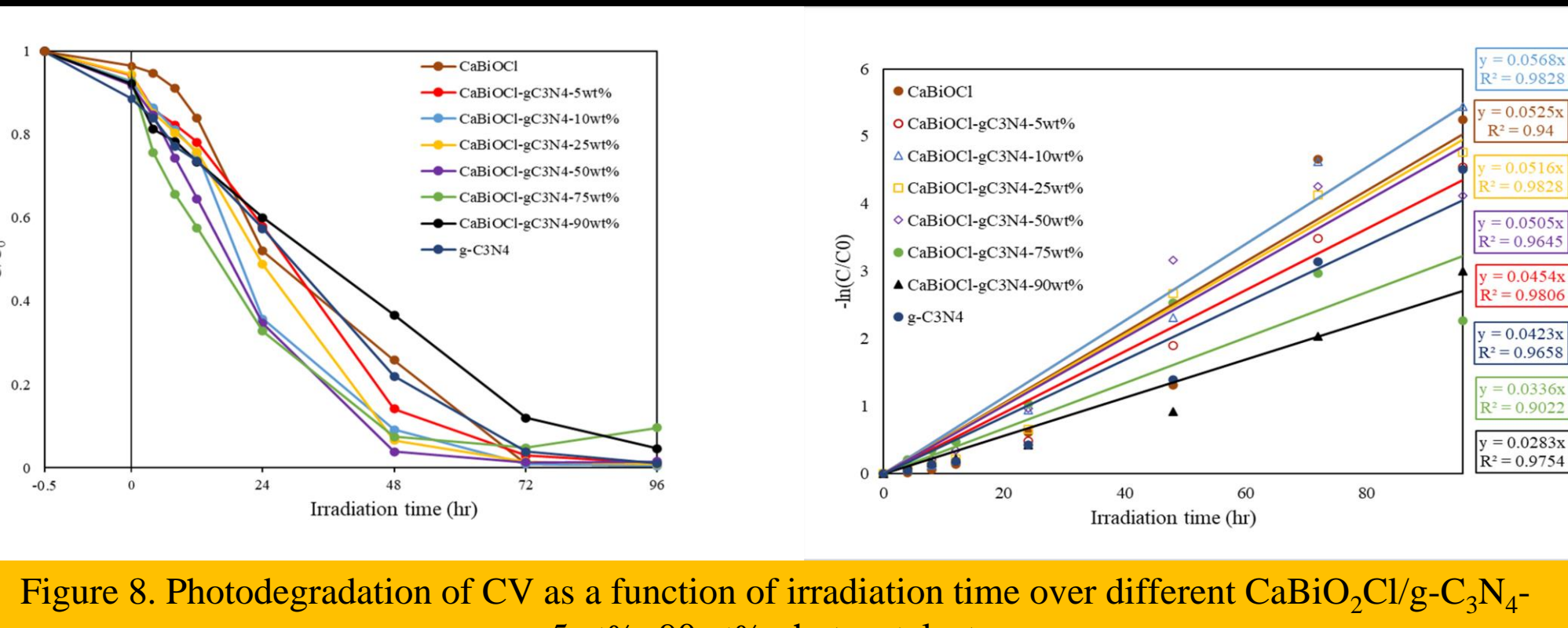


Figure 8. Photodegradation of CV as a function of irradiation time over different $\text{CaBiO}_2\text{Cl/g-C}_3\text{N}_4$ -5wt%-90wt% photocatalysts.

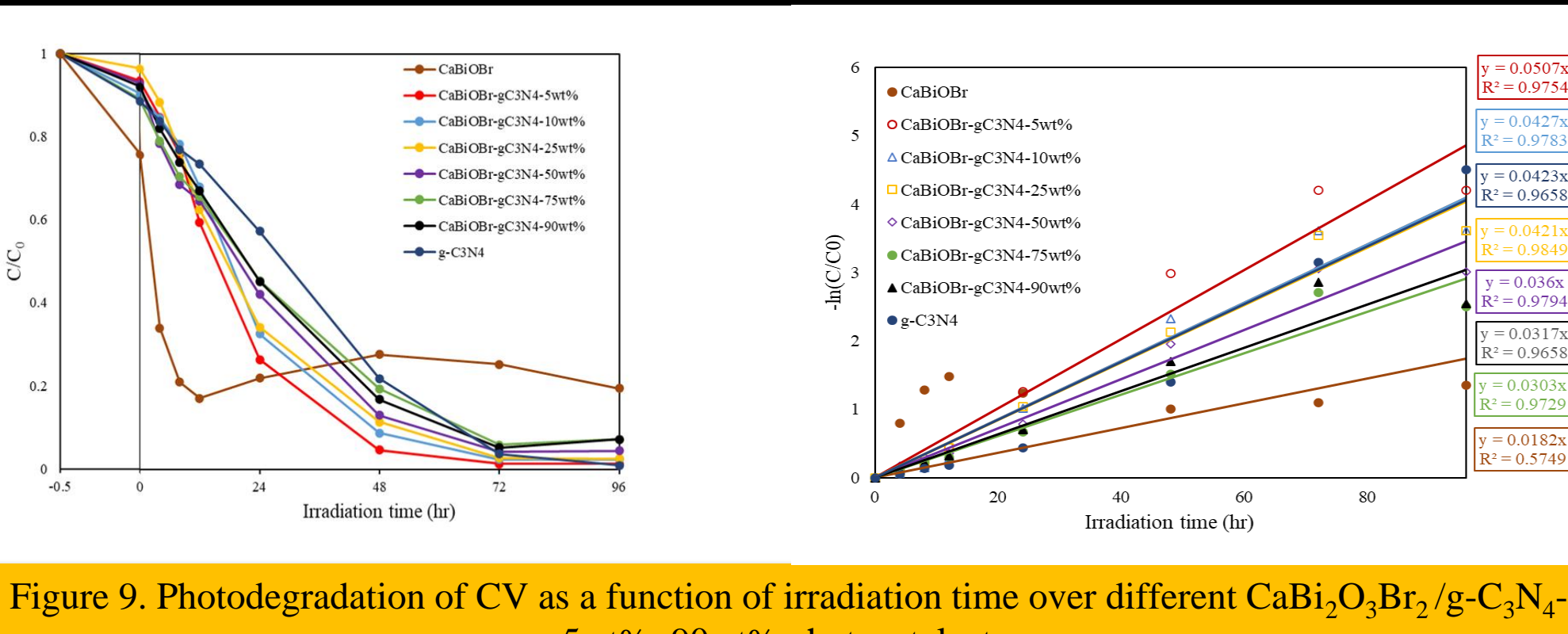


Figure 9. Photodegradation of CV as a function of irradiation time over different $\text{CaBi}_2\text{O}_3\text{Br}_2/\text{g-C}_3\text{N}_4$ -5wt%-90wt% photocatalysts.

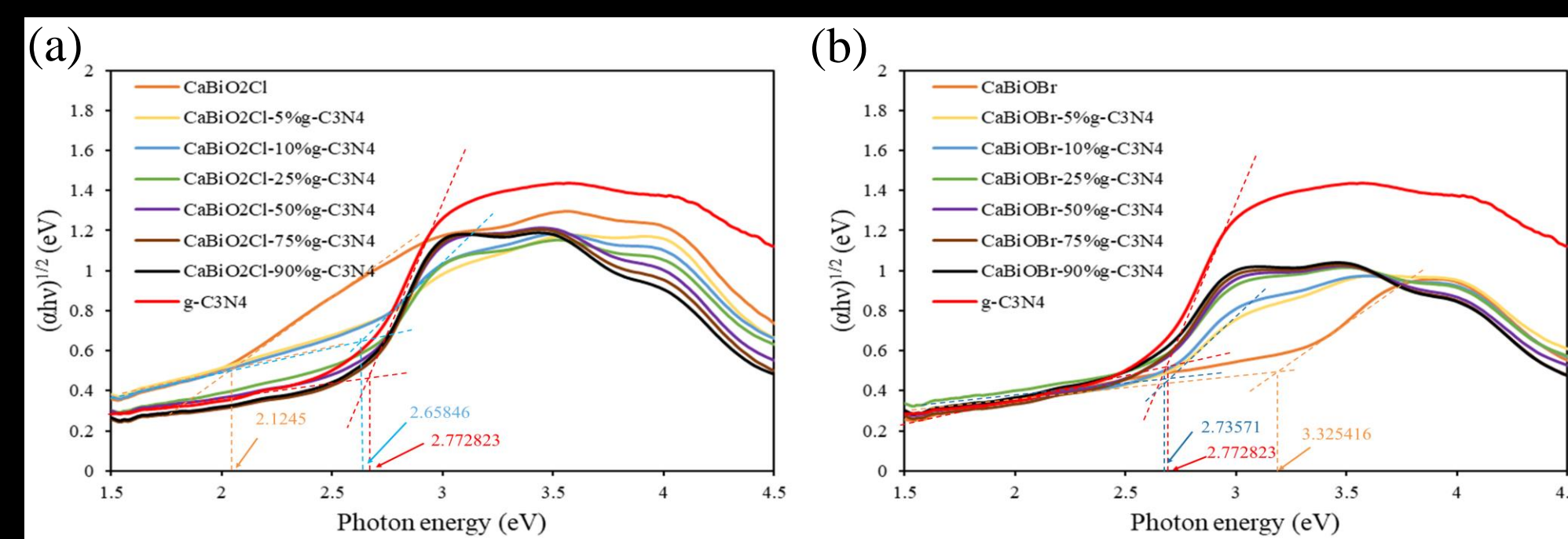


Figure 10. UV-vis absorption spectra of (a) $\text{CaBiO}_2\text{Cl/g-C}_3\text{N}_4$ -5wt%-90wt% and (b) $\text{CaBi}_2\text{O}_3\text{Br}_2/\text{g-C}_3\text{N}_4$ -5wt%-90wt% photocatalysts.

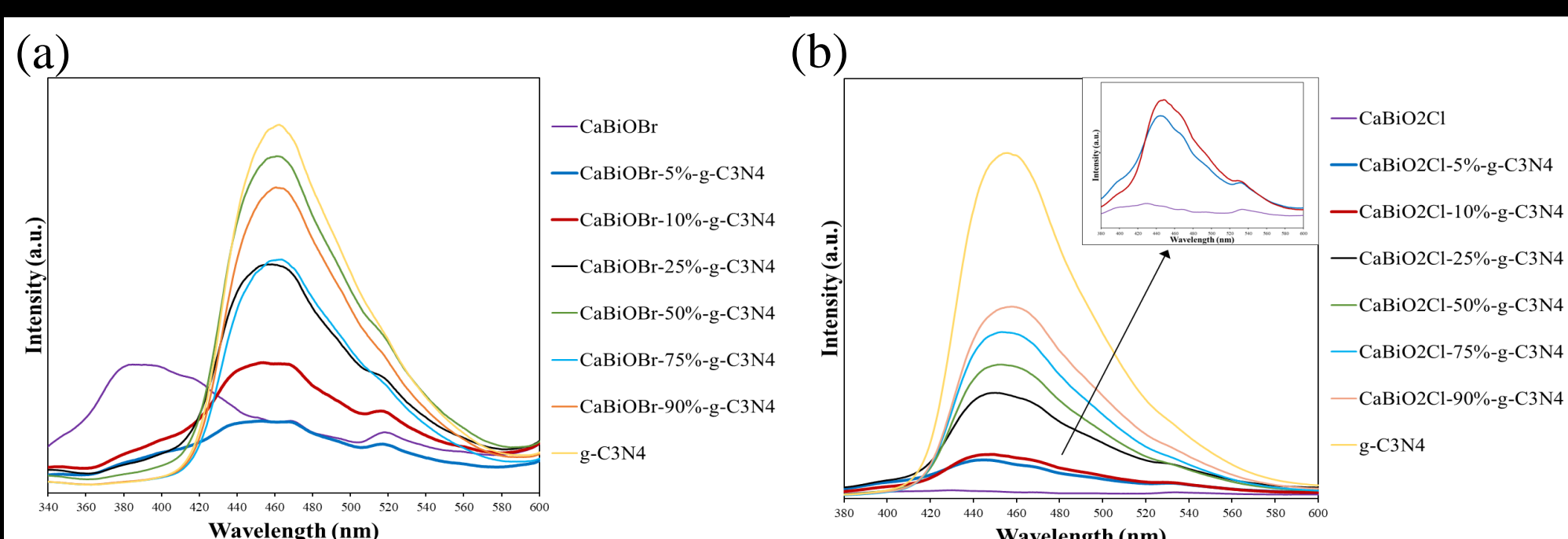


Figure 11. Photoluminescence spectra of (a) $\text{CaBiO}_2\text{Cl/g-C}_3\text{N}_4$ -5wt%-90wt% and (b) $\text{CaBi}_2\text{O}_3\text{Br}_2/\text{g-C}_3\text{N}_4$ -5wt%-90wt% photocatalysts.

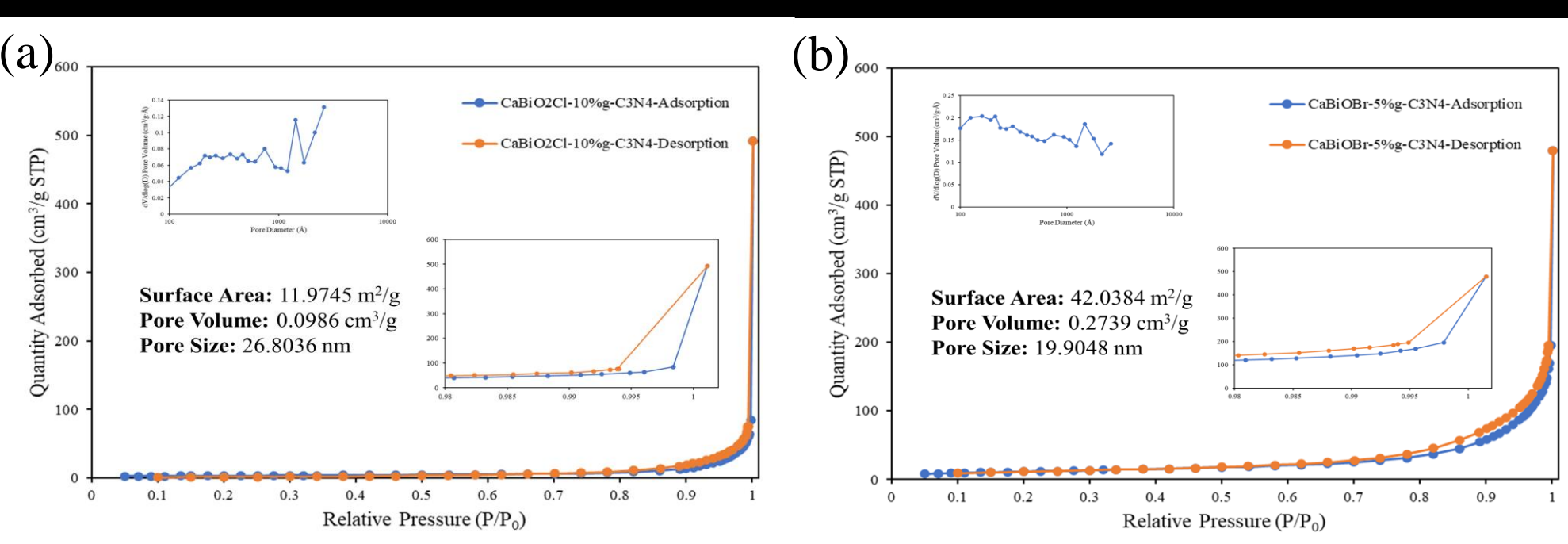


Figure 12. N_2 adsorption isotherm and pore size distribution of (a) $\text{CaBiO}_2\text{Cl/10wt\%-g-C}_3\text{N}_4$ and (b) $\text{CaBi}_2\text{O}_3\text{Br}_2/5\text{wt\%-g-C}_3\text{N}_4$ photocatalysts.

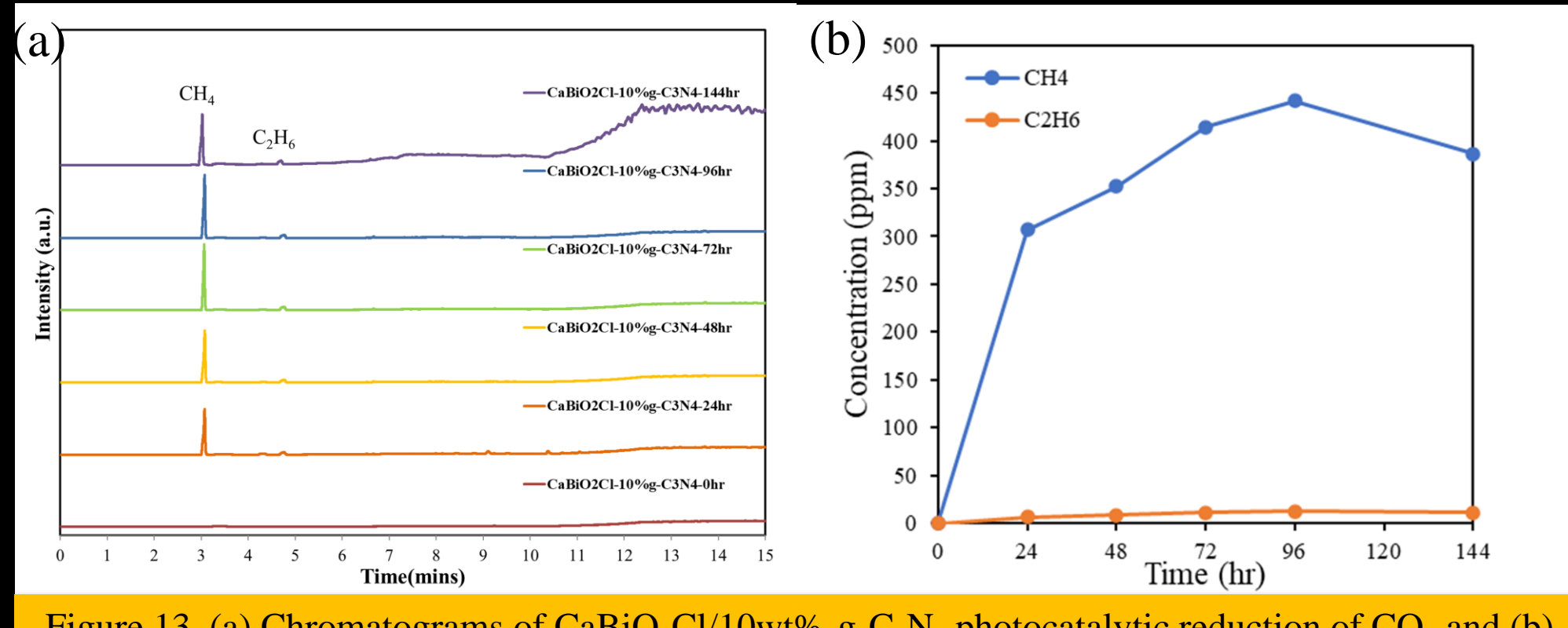


Figure 13. (a) Chromatograms of $\text{CaBiO}_2\text{Cl/10wt\%-g-C}_3\text{N}_4$ photocatalytic reduction of CO_2 and (b) as a function of irradiation time.

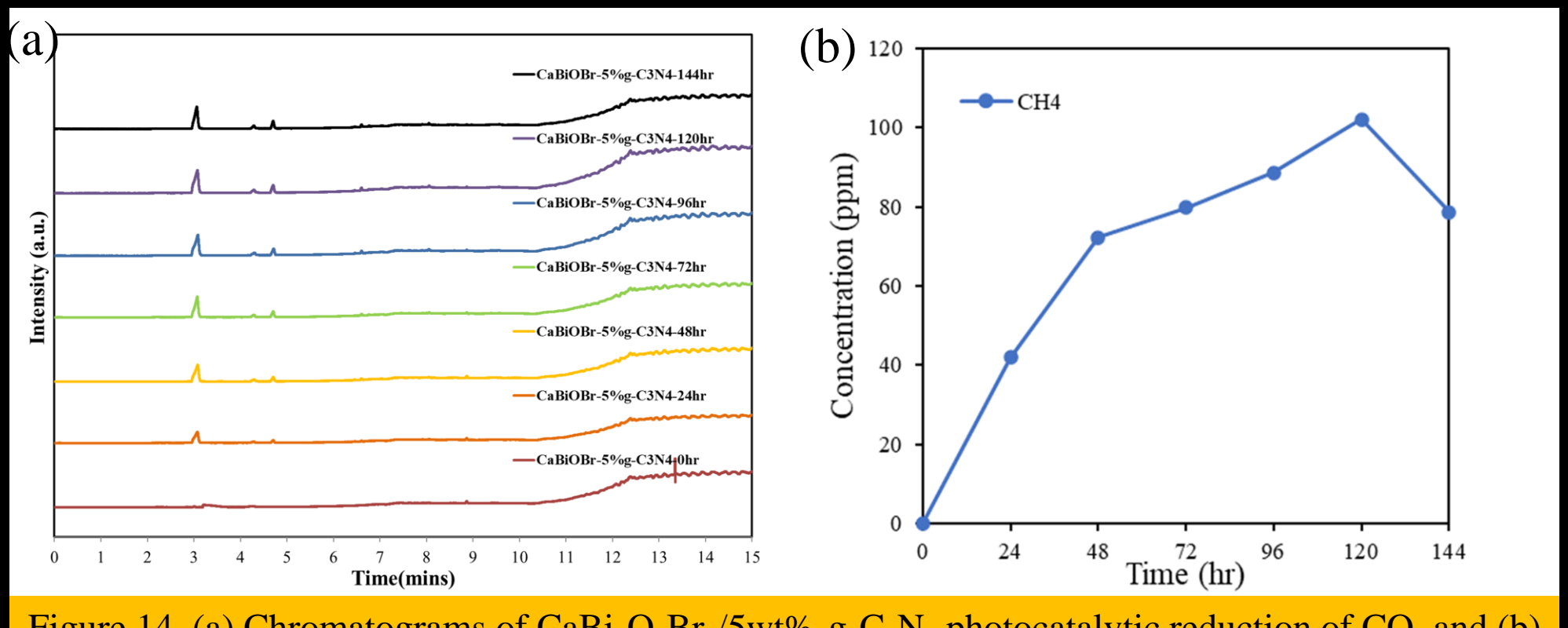


Figure 14. (a) Chromatograms of $\text{CaBi}_2\text{O}_3\text{Br}_2/5\text{wt\%-g-C}_3\text{N}_4$ photocatalytic reduction of CO_2 and (b) as a function of irradiation time.

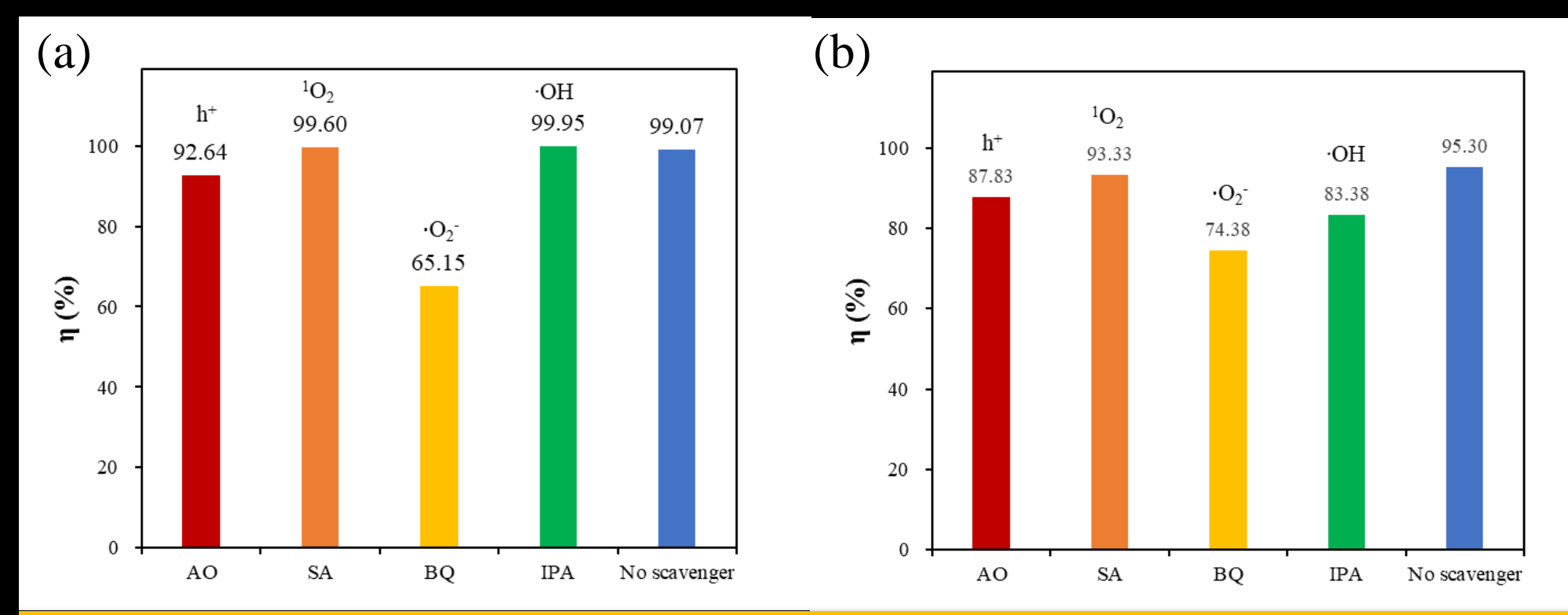


Figure 15. The dye concentration during photodegradation as a function of irradiation time observed in (a) $\text{CaBiO}_2\text{Cl/10wt\%-g-C}_3\text{N}_4$ and (b) $\text{CaBi}_2\text{O}_3\text{Br}_2/5\text{wt\%-g-C}_3\text{N}_4$ photocatalysts.

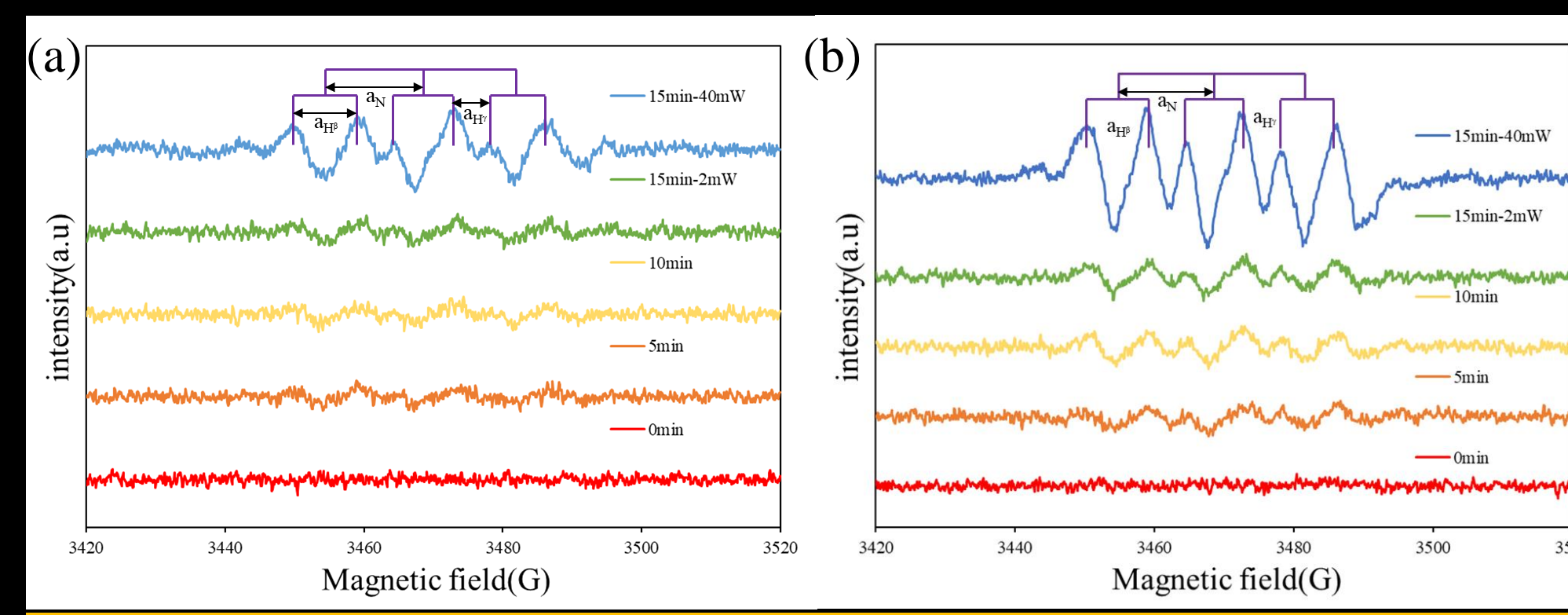


Figure 16. EPR spectra for DMPO- O_2 under visible light irradiation with (a) $\text{CaBiO}_2\text{Cl/g-C}_3\text{N}_4$ and (b) $\text{CaBi}_2\text{O}_3\text{Br}_2/\text{g-C}_3\text{N}_4$.

Table 1. Percent yield and Selectivity of CO_2 reduction.			
Sample	CaBiO_2Cl	$\text{g-C}_3\text{N}_4$	$\text{CaBiO}_2\text{Cl/g-C}_3\text{N}_4$
percent yield ($\mu\text{mol}\cdot\text{g}^{-1}\cdot\text{h}^{-1}$)	0.3331	0.1020	0.5652
CH_4 Selectivity (%)	88.28	99.88	94.52

Sample	$\text{CaBi}_2\text{O}_3\text{Br}_2$	$\text{g-C}_3\text{N}_4$	$\text{CaBi}_2\text{O}_3\text{Br}_2/\text{g-C}_3\text{N}_4$
percent yield ($\mu\text{mol}\cdot\text{g}^{-1}\cdot\text{h}^{-1}$)	0.1586	0.1020	0.1044
CH_4 Selectivity (%)	100	100	100

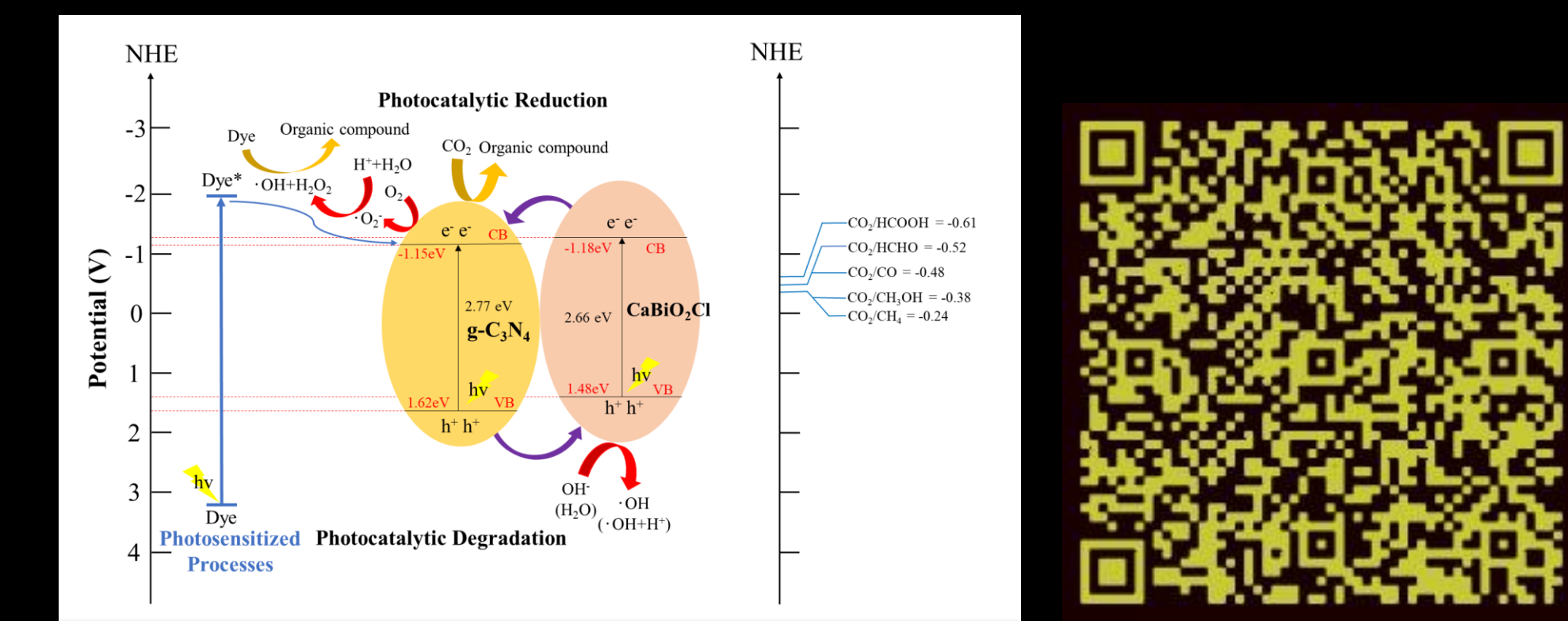


Figure 17. The band structure diagram of $\text{CaBiO}_2\text{Cl/g-C}_3\text{N}_4$ photocatalysts